

Low-temperature evolution of the modulated magnetic structure in the ferroelectric antiferromagnet BiFeO_3

I. Sosnowska and R. Przeniosła

Institute of Experimental Physics, Faculty of Physics, University of Warsaw, Hoża 69, PL 00-681 Warsaw, Poland

(Received 12 July 2011; revised manuscript received 9 August 2011; published 3 October 2011)

High-resolution time-of-flight neutron diffraction studies of the magnetic ordering in the multiferroic BiFeO_3 are presented. Our results show that the cycloidal modulated ordering proposed earlier [I. Sosnowska, T. Peterlin-Neumaier, and E. Steichele, *J. Phys. C* **15**, 4835 (1982)] is stable between 10 and 295 K. The concept of the anharmonic character of the magnetic modulation in BiFeO_3 that was used for the interpretation of NMR, Raman, and THz spectroscopy studies of BiFeO_3 is discussed. The influence of the anharmonic modulation on the magnetic contributions to the BiFeO_3 neutron diffraction patterns is presented. Our experimental data can be described by assuming anharmonic effects with $m < 0.25$. We propose a method for the anharmonicity strength evaluation based on neutron diffraction data.

DOI: [10.1103/PhysRevB.84.144404](https://doi.org/10.1103/PhysRevB.84.144404)

PACS number(s): 75.47.Lx, 75.85.+t, 75.50.Ee, 77.84.Bw

I. INTRODUCTION

The ferroelectric antiferromagnet BiFeO_3 is a subject of intensive studies—see, e.g., the reviews.^{1–5} For practical applications it is important to have a multiferroic material possessing the magnetoelectric effect (ME) at room temperature (RT). So far, to the best of our knowledge, there is only one such material, BiFeO_3 . The technical applications of this material are manifold, e.g., recently it was shown that BiFeO_3 could be applied in cancer medical treatments.⁶

The magnetic structure of BiFeO_3 is, in the first approximation, antiferromagnetic (G -type magnetic ordering), as it was determined by Kiselev *et al.*⁷ in the 1960's. High-resolution time-of-flight neutron diffraction was used for magnetic ordering studies of BiFeO_3 (Ref. 8) in the 1980's. It was found that the G -type antiferromagnetic structure of BiFeO_3 at RT is subjected to a long-range modulation of cycloidal type with the spiral length $L = 62.0 \pm 2.0$ nm. It was determined that the spiral direction is $[1, 1, 0]_{\text{hex}}$ and the Fe^{3+} spin rotation plane is $(-110)_{\text{hex}}$ (in the hexagonal setting). The paper⁸ claims also that the cycloidal magnetic ordering in BiFeO_3 is observed at 77 K. Further studies have shown that the cycloidal magnetic ordering is stable and does not change its character up to the Néel temperature.⁹ Recently these results were confirmed by single-crystal BiFeO_3 neutron diffraction studies.¹⁰

The theoretical description of the magnetic interactions in BiFeO_3 is often limited to the collinear antiferromagnetic spin arrangement only. An earlier paper explaining the modulated structure in BiFeO_3 was based on the anisotropic relativistic interactions and their contribution to the creation of the cycloidal magnetic ordering.¹¹ The anisotropic relativistic interactions are responsible for the magnetic cycloidal spiral experimentally found in BiFeO_3 .⁸ Different approaches were used later, but this problem needs further efforts. The Dzyaloshinskii-Moriya interactions are in general responsible for this complicated magnetic moment arrangement in BiFeO_3 .

There is no controversy concerning the crystal structure of BiFeO_3 —see, e.g., the review in Ref. 12. The crystal structure is described with the space group $R3c$ and it is a double-perovskite-like unit cell. The BiFeO_3 crystal structure can be also described by using the pseudocubic setting as explained in Ref. 13. Neutron powder diffraction studies of the crystal

structure of BiFeO_3 done at temperatures from 4 to 700 K did not show any structural phase transitions.^{14,15}

Low-temperature NMR BiFeO_3 studies by Zaleskii *et al.*¹⁶ were interpreted by assuming that the cycloidal Fe^{3+} magnetic moment ordering is described with an anharmonic cycloidal modulation. The harmonic cycloidal magnetic ordering at RT is described with the $\sin(qx)$ and $\cos(qx)$ functions. Below RT Zaleskii *et al.*¹⁶ propose to use the Jacobi $\text{sn}(qx, m)$ and $\text{cn}(qx, m)$ functions. According to Ref. 16, the degree of anharmonicity in BiFeO_3 (given by the parameter m) increases with decreasing temperature. The cycloidal modulation described with Jacobi functions is often called “anharmonic” because $\text{sn}(qx, m)$ has many nonzero odd harmonic terms in its Fourier expansion.

There is a set of recent papers which report several anomalies in the physical properties of BiFeO_3 at temperatures below RT (see, e.g., the review in Ref. 17). These anomalies include Raman spectroscopy,^{17–19} dielectric measurements,²⁰ and THz spectroscopy.²¹ One of the common explanations of these anomalies is attributed to changes of the cycloidal magnetic structure (e.g., changes of the spin ordering plane, the so-called reorientation transitions). Another explanation of the anomalies was attributed to the changes of the degree of anharmonicity of the magnetic ordering.¹⁶ In other words, anomalies of unknown origin are explained by assuming “magnetic reorientations,” “magnetic anharmonicities,” or in general “magnetic phase transitions” without firm justification.

Recent BiFeO_3 NMR studies by Pokatilov and Sigov²² have shown that the results from Zaleskii *et al.*¹⁶ included important artifacts mainly due to the high ^{57}Fe isotope content in their BiFeO_3 samples. Pokatilov and Sigov performed NMR studies on BiFeO_3 samples with different ^{57}Fe content and they concluded²² “. . . BiFeO_3 at $T = 4.2$ K has a spatial spin modulated cycloid magnetic structure rather than an anharmonic (disturbed) spin modulated cycloid structure.” To the best of our knowledge, the paper²² has not been cited so far and many authors still use the argument of “changes in anharmonicity” of the cycloidal ordering to describe their results.

Recently a unique insight on low-temperature BiFeO_3 magnetic ordering was obtained from single-crystal neutron

diffraction.¹⁰ The authors of Ref. 10 do not observe any changes in the magnetic structure for $T < 300$ K, except for a slow and gradual change of the cycloid periodicity. The main conclusion of the paper¹⁰ is that the anomalies previously observed in Raman^{17–19} and dielectric measurements²⁰ are not related to spin-reorientation transitions. The authors of Ref. 10 reported some small effects of anharmonicity of the cycloidal magnetic ordering at 5 K.

In the present paper we present high-resolution BiFeO₃ neutron powder diffraction studies performed below RT. The present studies are an extension of our earlier work²³ performed at 4 and 300 K only. We focus on the possibility of the detection of the anharmonic cycloidal modulation by using high-resolution neutron diffraction measurements.

II. EXPERIMENT

Neutron powder diffraction measurements of BiFeO₃ have been performed at the high-resolution time-of-flight (TOF) neutron diffractometer HRPD at the ISIS facility.²⁴ The polycrystalline powder BiFeO₃ sample was placed in a 5-mm-thick flat vanadium container inside a helium-flow cryostat. Data were recorded at temperatures 10, 135, 195, 230, and 295 K. The measurements were done for the interplanar d -spacing range of 4.3–4.7 Å, i.e., in the region with the most intense magnetic satellites around (101) and (003)—see Fig. 2 below and Table I. The measurements were also performed for the interplanar d -spacing range of 1.0–2.5 Å, in order to refine the BiFeO₃ lattice parameters. The measured neutron diffraction intensities have been normalized and corrected for detector efficiency effects using previously recorded vanadium calibration data.

III. RESULTS

The section of the BiFeO₃ reciprocal lattice at $l = 1$ plane in the hexagonal setting is shown in Fig. 1. The

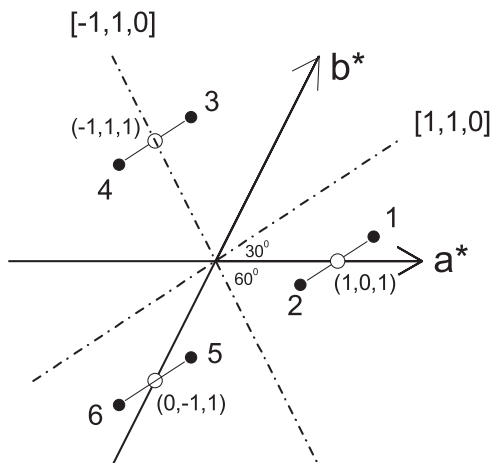


FIG. 1. Section of the BiFeO₃ reciprocal lattice corresponding to the $l = 1$ plane in the hexagonal setting. The hexagonal reciprocal axes a^* and b^* are shown. There are six magnetic satellite positions (solid symbols) located on both sides of the Bragg positions $(1,0,1)_{\text{hex}}$, $(\bar{1},1,1)_{\text{hex}}$, and $(0,\bar{1},1)_{\text{hex}}$ (open symbols). The indexing of the satellites labeled as $L_1, L_2, C_1, C_2, R_1, R_2$ is given in Table I.

TABLE I. List of selected magnetic satellite Bragg peaks observed in BiFeO₃ given in both hexagonal and pseudocubic indexing. The value of the interplanar distance d (Å) is also shown.

| No. | Label | Hexagonal | Pseudocubic | d (Å) |
|-----|-------|--------------------------------|--|---------|
| 1 | L_1 | $(1 + \delta, \delta, 1)$ | $(\frac{1}{2} + \delta, -\frac{1}{2} - \delta, \frac{1}{2})$ | 4.53 |
| 2 | L_2 | $(-\delta, -1 - \delta, 1)$ | $(-\frac{1}{2} - \delta, \frac{1}{2} + \delta, \frac{1}{2})$ | 4.53 |
| 3 | C_1 | $(-1 + \delta, 1 + \delta, 1)$ | $(\frac{1}{2} + \delta, \frac{1}{2} - \delta, -\frac{1}{2})$ | 4.55 |
| 4 | C_2 | $(-1 - \delta, 1 - \delta, 1)$ | $(\frac{1}{2} - \delta, \frac{1}{2} + \delta, -\frac{1}{2})$ | 4.55 |
| 5 | R_1 | $(1 - \delta, -\delta, 1)$ | $(\frac{1}{2} - \delta, -\frac{1}{2} + \delta, \frac{1}{2})$ | 4.58 |
| 6 | R_2 | $(\delta, -1 + \delta, 1)$ | $(-\frac{1}{2} + \delta, \frac{1}{2} - \delta, \frac{1}{2})$ | 4.58 |
| 7 | | $(\delta, \delta, 3)$ | $(\frac{1}{2} + \delta, \frac{1}{2} - \delta, \frac{1}{2})$ | 4.62 |
| 8 | | $(-\delta, -\delta, 3)$ | $(\frac{1}{2} - \delta, \frac{1}{2} + \delta, \frac{1}{2})$ | 4.62 |

modulated cycloidal magnetic ordering model described in BiFeO₃ (Ref. 8) gives magnetic satellite peaks located in this plane around the Bragg positions $(1,0,1)_{\text{hex}}$, $(\bar{1},1,1)_{\text{hex}}$, and $(0,\bar{1},1)_{\text{hex}}$ (see Fig. 1). The satellites' labeling is coherent with the notation used in our previous neutron powder diffraction studies,²³ where the satellite peaks were labeled as “left” (L), “central” (C), and “right” (R) due to their positions on the neutron diffraction pattern shown as a function of interplanar distance d (see, e.g., Fig. 2 below). The satellites labeled as L_1 and L_2 contribute to the left peak, C_1 and C_2 to the central peak, and R_1 and R_2 to the right peak. The indexing of these magnetic satellites is given in Table I. There are numerous diffraction studies of BiFeO₃ in which the pseudocubic setting is used, so we show the indexing in both pseudocubic and hexagonal systems in Table I.

The cycloid propagation vector $\mathbf{q} = (\delta, \delta, 0)_{\text{hex}}$ in hexagonal setting was first determined in Ref. 8 with $\delta = 0.0045$. In order to compare our results with the recent BiFeO₃ single-crystal neutron diffraction studies¹⁰ we use the pseudocubic setting with the propagation vector $\mathbf{q} = (\delta, -\delta, 0)_{\text{pc}}$. The magnetic moments remain in the plane span by the propagation vector direction $[1,1,0]_{\text{hex}}$ and the c -axis $[0,0,1]_{\text{hex}}$.⁸ In the pseudocubic setting these directions correspond to $[1,-1,0]_{\text{pc}}$ and $[1,1,1]_{\text{pc}}$, respectively.

The BiFeO₃ neutron powder diffraction patterns are shown in Fig. 2. The results shown in Fig. 2 cover the region of magnetic satellites listed in Table I. We observe a gradual shift of the satellite peak positions due to the BiFeO₃ thermal expansion.

The four magnetic satellite peak positions were fitted with pseudo-Voigt functions and a linear background as already described in Ref. 23. The $1.0 \text{ \AA} < d < 2.5 \text{ \AA}$ neutron diffraction data (not shown) was analyzed with the Rietveld method by using the FULLPROF program²⁵ in order to follow the temperature dependence of the lattice parameters. The temperature dependence of the magnetic modulation length λ and the propagation vector parameter δ obtained from our experimental data are shown in Figs. 3(a) and 3(b), respectively. The trend of δ versus temperature is similar to that obtained from BiFeO₃ single-crystal studies,¹⁰ but the absolute values of δ are different.

The circular cycloid magnetic ordering model proposed in Ref. 8 assumes that the Fe³⁺ magnetic moment has two perpendicular components: M_x , which is parallel to the

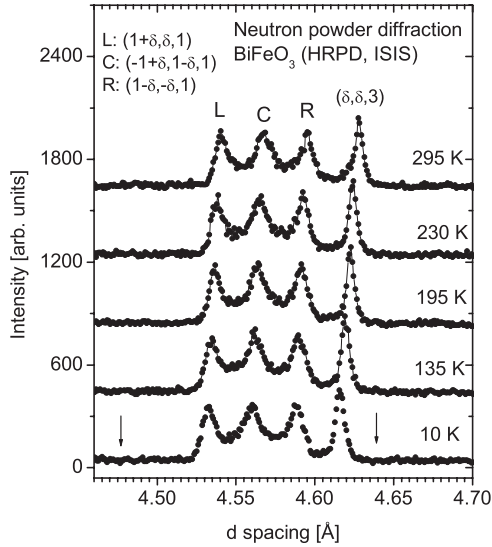


FIG. 2. Neutron powder diffraction pattern of BiFeO₃ measured at several temperatures between 10 and 295 K. The symbols L,C,R correspond to the labeling given in Table I. Vertical arrows show the positions of the third-order satellites $(1 - 3\delta, -3\delta, 1)_{\text{hex}}$ and $(1 + 3\delta, +3\delta, 1)_{\text{hex}}$ expected for the anharmonic model at low temperature.

propagation vector $\mathbf{q} = (\delta, \delta, 0)_{\text{hex}}$, i.e., along the x axis, and M_z , which is parallel to the $[0, 0, 1]_{\text{hex}}$, i.e., along the z axis. The cycloidal modulation is described as⁸

$$M_x = M_0 \cos(qx), \quad (1)$$

$$M_y = 0, \quad (2)$$

$$M_z = M_0 \sin(qx), \quad (3)$$

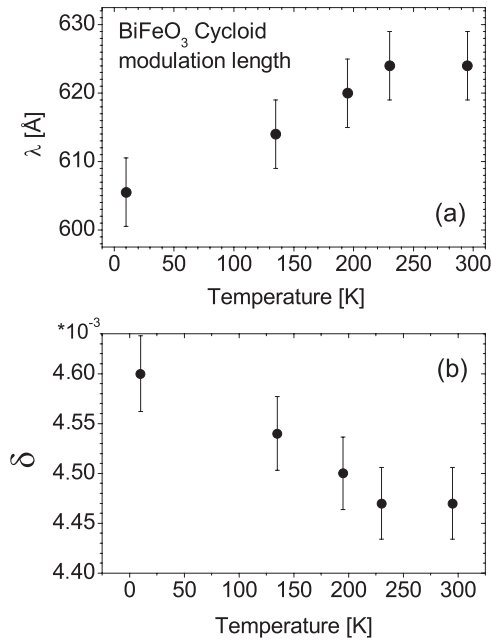


FIG. 3. (a) Temperature dependence of the magnetic cycloid modulation length L . (b) Temperature dependence of the propagation vector index δ . The results of (a) and (b) are obtained from the magnetic satellite peak positions determined from BiFeO₃ neutron diffraction patterns shown in Fig. 2.

where q is the propagation vector \mathbf{q} length and x is the position along the x axis. M_0 is the amplitude of the ordered Fe³⁺ magnetic moment. Please note that $M_x^2 + M_z^2 = M_0^2$.

The BiFeO₃ NMR studies have shown anomalies which could be explained by using an anharmonic cycloidal magnetic ordering¹⁶ where the sine and cosine are replaced by the Jacobi sn and cn functions. The spin rotation plane and the modulation direction are the same as in the harmonic model and the Fe³⁺ magnetic ordering is given by

$$M_x = M_0 \text{cn}[(4K(m)/\lambda)x, m], \quad (4)$$

$$M_y = 0, \quad (5)$$

$$M_z = M_0 \text{sn}[(4K(m)/\lambda)x, m], \quad (6)$$

where x is the position along the x axis, $K(m)$ is the complete elliptic integral of the first kind, λ is the modulation length (~ 620 Å), and m is the Jacobi anharmonicity parameter ($0 \leq m \leq 1$). For $m = 0$ the Jacobi $\text{sn}(x, m) = \sin(x)$. At any position we obtain a constant magnetic moment value M_0 for any m : $M_x^2 + M_z^2 = M_0^2$.

The intensity signal shown in Fig. 2 is equal to

$$I_{hkl}^{\text{TOF}} \propto d^4 j |F_{hkl}|^2, \quad (7)$$

where d is the interplanar distance and j is the multiplicity factor for the peak indexed as (h, k, l) . The neutron diffraction patterns with I_{hkl}^{TOF} have been analyzed with the Rietveld method by using FULLPROF.²⁵ In order to compare our experimental results with calculations and also with results of single-crystal studies, e.g., see Ref. 10, we analyze the corrected intensities I_{hkl} :

$$I_{hkl} \propto j |F_{hkl}|^2. \quad (8)$$

Our experimental intensities I_{hkl}^{TOF} were corrected by using the formula $I_{hkl} = I_{hkl}^{\text{TOF}}/d^4$.

We have also performed model calculations of the expected magnetic Bragg peak intensities I_{hkl} . The calculations were done by using the magnetic scattering cross-section formulas for modulated orderings.²⁶ In the calculations we used the Fe³⁺ magnetic form factor.²⁷ We assumed that the magnetic moment amplitude $M_0 = 1$ for any value of m . The magnetic cross section has been calculated for all the satellites listed in Table I.

The calculated neutron diffraction intensities are shown in Figs. 4(a)–4(d). I^1 and I^3 denote the intensities of the first- and third-order satellites. For the harmonic modulation $m = 0$ there is no third-order satellite intensity $I^3 = 0$. For all the satellites we observe an increase of the calculated third-order satellite intensity I^3 with m . For the extreme case ($m = 1$) of rectangular antiphase domain ordering (not shown) we obtain a value of $I^1/I^3 = 9$ for the $L_1, L_2, C_1, C_2, R_1, R_2$ satellites given in Table I, in agreement with the results given by Bacon (see Fig. 163 in Ref. 28). The value of $I^1/I^3 = 500$ reported in recent BiFeO₃ single-crystal neutron diffraction studies¹⁰ corresponds to $m = 0.50$, as shown by the vertical dotted line in Figs. 4(a)–4(d). The weak third-order satellites are difficult to observe, as one can notice in Fig. 4(a) in Ref. 10. Our neutron powder diffraction data (see Fig. 2) has no sufficient statistical accuracy to detect such weak third-order satellite intensities.

It is important to note that one can obtain information about the anharmonic magnetic modulation by analyzing the change

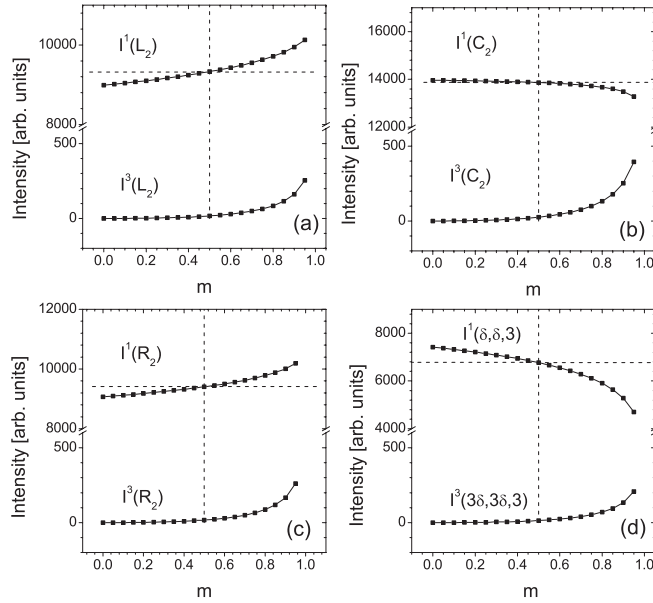


FIG. 4. Calculated neutron diffraction intensities of first-order I^1 and third-order I^3 magnetic satellite peaks for several values of the anharmonicity parameter m . The intensity of the satellites L_2 , C_2 , and R_2 (see also Fig. 1) is given in (a)–(c), respectively. The intensity of the satellites $(\delta, \delta, 3)$ is given in (d). The vertical dotted line indicates $m = 0.50$ (see text).

of the intensity of first-order satellites I^1 with m , as shown in Figs. 4(a)–4(d). For the satellites C_1, C_2 [Fig. 4(b)] the scattering vector is almost perpendicular to the spin plane, making an angle equal to 19.4° with the vector normal to the spin plane \mathbf{n} . There is a very weak change of $I^1(C_2)$ with m . For the satellites $(\delta, \delta, 3)$ [Fig. 4(d)] the scattering vector lies almost within the spin plane and there is an important decrease of $I^1(\delta, \delta, 3)$ with m . For the satellites L_1, L_2 and R_1, R_2 [Figs. 4(a) and 4(c)] the scattering vector makes an angle of $\sim 61.8^\circ$ with \mathbf{n} and there is an increase of $I^1(L_2)$ and $I^1(R_2)$ with m .

In order to compare our experimental data with calculations we have estimated the intensity ratio $A = I_{\delta, \delta, 3} / (I_L + I_C + I_R)$, as discussed in Ref. 23. The fit of pseudo-Voigt functions does not give sufficiently good agreement with the experimental peak shapes. We determined the total intensity of the L , C , and R satellite peaks together and the intensity of the $(\delta, \delta, 3)$ peak with a subtraction of a linear background. The values of ratio A determined from the experimental data are shown in Fig. 5(a). The values of ratio A calculated from intensity values given in Fig. 4 are shown in Fig. 5(b). For the harmonic cycloidal ordering (i.e., $m = 0$) we obtain $A = 0.232$, in agreement with Ref. 8. The calculated values of A decrease with increasing m . For $m = 0.50$ reported from BiFeO₃ single-crystal studies¹⁰ at 5 K, $A = 0.208$, i.e., one

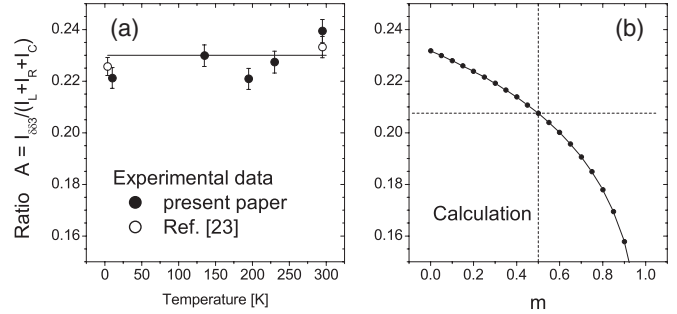


FIG. 5. (a) Temperature dependence of the magnetic first-order satellite intensity ratio A (see text) determined from experimental data in the present paper (solid symbols) and our earlier work (Ref. 23) (open symbols). (b) Calculated values of the ratio A as a function of the anharmonicity parameter m .

can expect a relative change of A by 11.5% between 5 K and RT [see Fig. 5(b)]. Our experimental data fluctuates at approximately $A = 0.23$, but we do not see any temperature trend [see Fig. 5(a)]. The fluctuation amplitude corresponds to changes in the anharmonicity parameter of no more than $m = 0.25$.

IV. CONCLUSIONS

Our high-resolution neutron powder diffraction data provides important information about the temperature evolution of the magnetic ordering in BiFeO₃. Our data does not support the anharmonic modulation model with $m = 0.50$ proposed from BiFeO₃ single-crystal studies at $T = 4$ K.¹⁰ According to our experimental data the values of the anharmonicity parameter should not exceed 0.25. The published interpretations of observed temperature changes in NMR,¹⁶ Raman,¹⁹ and THz spectra²¹ based on temperature changes of magnetic order in BiFeO₃ need further consideration. We propose a test of the validity of the anharmonic model based on measurements of the first-order magnetic satellites of BiFeO₃ at low temperatures. Such measurements could be performed with single-crystal neutron diffraction, see, e.g., Refs. 10 and 29–31, and compared with calculations presented in Figs. 4 and 5.

ACKNOWLEDGMENTS

Thanks are due to A. Daoud-Aladine (ISIS) for help as the local contact in the neutron diffraction measurements. This research project has been supported by the European Commission under the 7th Framework Programme through the Key Action: Strengthening the European Research Area, Research Infrastructures, Contracts No. CP-CSA-INFRA-2008-1.1.1 and No. 226507-NMI3. Thanks are due to the Ministry of Science and Higher Education (Poland) for funding.

¹N. A. Spaldin, S.-W. Cheong, and R. Ramesh, *Phys. Today* **63** (10), 38 (2010).

²C. Ederer and N. A. Spaldin, *Phys. Rev. B* **71**, 060401 (2005).

³W. Eerenstein, N. D. Mathur, and J. F. Scott, *Nature (London)* **442**, 759 (2006).

⁴M. Fiebig, *J. Phys. D* **38**, R123 (2005).

- ⁵N. A. Hill, *J. Phys. Chem. B* **104**, 6694 (2000).
- ⁶Z. Dai, Y. Fujita, and Y. Akishige, *Mater. Lett.* **65**, 2036 (2011).
- ⁷S. V. Kiselev, R. Ozerov, and G. S. Zhanov, *Sov. Phys. Dokl.* **7**, 742 (1963).
- ⁸I. Sosnowska, T. Peterlin-Neumaier, and E. Steichele, *J. Phys. C* **15**, 4835 (1982).
- ⁹I. Sosnowska, M. Loewenhaupt, W. I. F. David, and R. M. Ibberson, *Physica B* **180–181**, 117 (1992).
- ¹⁰M. Ramazanoglu, W. Ratcliff II, Y. J. Choi, S. Lee, S.-W. Cheong, and V. Kiryukhin, *Phys. Rev. B* **83**, 174434 (2011).
- ¹¹I. Sosnowska and A. K. Zvezdin, *J. Magn. Magn. Mater.* **140**, 167 (1995).
- ¹²I. Sosnowska, *J. Microsc.* **236**, 109 (2009).
- ¹³H. D. Megaw and C. N. W. Darlington, *Acta Crystallogr. Sect. A* **31**, 161 (1975).
- ¹⁴P. Fischer, M. Połomska, I. Sosnowska and M. Szymański, *J. Phys. C* **13**, 1931 (1980).
- ¹⁵A. Palewicz, R. Przeniosło, I. Sosnowska and A. Hewat, *Acta Crystallogr. Sect. B* **63**, 537 (2007).
- ¹⁶A. Zalesskii, A. Frolov, T. Khimich, A. Bush, V. Pokatilov, and A. Zvezdin, *Europhys. Lett.* **50**, 547 (2000).
- ¹⁷G. Catalan and J. F. Scott, *Adv. Mater.* **21**, 2463 (2009).
- ¹⁸M. Cazayous, Y. Gallais, A. Sacuto, R. de Sousa, D. Lebeugle, and D. Colson, *Phys. Rev. Lett.* **101**, 037601 (2008).
- ¹⁹M. K. Singh, R. S. Katiyar, and J. F. Scott, *J. Phys. Condens. Matter* **20**, 252203 (2008).
- ²⁰S. A. T. Redfern, C. Wang, J. W. Hong, G. Catalan, and J. F. Scott, *J. Phys. Condens. Matter* **20**, 452205 (2008).
- ²¹D. Talbayev, S. A. Trugman, S. Lee, H. T. Yi, S.-W. Cheong, and A. J. Taylor, *Phys. Rev. B* **83**, 094403 (2011).
- ²²V. S. Pokatilov and A. S. Sigov, *JETP* **110**, 440 (2010).
- ²³R. Przeniosło, A. Palewicz, M. Regulski, I. Sosnowska, R. M. Ibberson, and K. S. Knight, *J. Phys. Condens. Matter* **18**, 2069 (2006); **23**, 279801 (2011) (corrigendum).
- ²⁴R. M. Ibberson, W. I. F. David, and K. S. Knight, Rutherford Appleton Laboratory Report No. RAL-92-031, 1992 (unpublished).
- ²⁵J. Rodriguez-Carvajal, *Physica B* **192**, 55 (1992).
- ²⁶G. L. Squires, *Introduction to the Theory of Thermal Neutron Scattering* (Cambridge University Press, Cambridge, UK, 1978), p. 153.
- ²⁷*International Tables for Crystallography* (Kluwer Academic, Dordrecht, 1995), Vol. C, p. 392.
- ²⁸G. E. Bacon, *Neutron Diffraction*, 3rd ed. (Clarendon, Oxford, UK, 1975), p. 269.
- ²⁹S. Lee, T. Choi, W. Ratcliff, R. Erwin, S.-W. Cheong, and V. Kiryukhin, *Phys. Rev. B* **78**, 100101(R) (2008).
- ³⁰J. Herrero-Albillos, G. Catalan, J. A. Rodriguez-Velamazan, M. Viret, D. Colson, and J. F. Scott, *J. Phys. Condens. Matter* **22**, 256001 (2010).
- ³¹D. Lebeugle, D. Colson, A. Forget, M. Viret, A. M. Bataille, and A. Goukasov, *Phys. Rev. Lett.* **100**, 227602 (2008).